Journal of Alloys and Compounds 705 (2017) 273–282

Contents lists available at ScienceDirect

Journal of Alloys and Compounds

journal homepage: http://www.elsevier.com/locate/jalcom

Influence of equal channel angular pressing temperature on texture, microstructure and mechanical properties of extruded AX41 magnesium

Tomáš Krajňák [a, b, *], Peter Minárik [a], Jitka Stráská [a], Jenő Gubicza [c], Kristián Máthis [a], Miloš Janeček [a]

[a] Charles University, Faculty of Mathematics and Physics, Ke Karlovu 3, 121 16 Praha 2, Czech Republic
[b] Institute of Physics, Slovak Academy of Sciences, Dúbravska cesta 9, 845 11 Bratislava, Slovakia
[c] Eötvös Loránd University, Department of Materials Physics, P.O.B. 32, Budapest, H-1518, Hungary

ARTICLE INFO

Article history:
Received 11 October 2016
Received in revised form
20 January 2017
Accepted 7 February 2017
Available online 11 February 2017

Keywords:
AX41 magnesium alloy
ECAP
EBSD
X-ray line profile analysis
Dislocation structure
Texture

ABSTRACT

The objective of this study is the investigation of the effect of temperature of equal channel angular pressing (ECAP) on the microstructure, texture and mechanical properties of AX41 magnesium alloy. ECAP processing was performed at temperatures of 220 °C and 250 °C up to 8 passes via route Bc. It was found that during ECAP processing at 250 °C a smaller number of passes was enough to achieve a homogeneous microstructure than at 220 °C. However, the final grain size obtained after 8 passes at 250 °C was only 4 μm which is larger than the value of 2.7 μm achieved at 220 °C. Moreover, a significant influence of the temperature of ECAP processing on the dislocation density and the crystallographic texture was observed. The proof stress of the sample processed by 8 passes at 250 °C was lower than that obtained at 220 °C. It can be attributed to the lower dislocation density, the larger grain size and the texture, which facilitates the basal slip.

1. Introduction

Current use of magnesium alloys is mainly based on Mg-Al alloys due to their excellent castability, corrosion resistance and good mechanical properties (combination of enhanced strength and ductility) at room temperature (RT). As magnesium alloys generally suffer from poor creep resistance and strength at temperatures above 120 °C, their use in automotive powertrain applications, particularly for producing engine parts or transmission cases is still limited.

In order to improve mechanical properties at elevated temperatures several new Mg-Al die cast alloys based on rare earth, calcium or silicon additions were developed [1–4]. The enhanced creep strength of these alloys is caused by the formation of new, thermally stable intermetallic phases. By addition of Ca, as the cheaper and lighter counterpart to the rare earth metals, the new ternary magnesium alloys of AX (Mg-Al-Ca) series were developed. These materials exhibit improved high temperature strength and creep resistance due to the formation of heat resistant Mg_2Ca and Al_2Ca precipitates [5–7].

The poor formability and low ductility of magnesium alloys at RT, caused by their hexagonal close-packed (HCP) crystal structure, further limits their practical applications. Microstructural refinement obtained by severe plastic deformation (SPD) was found to be beneficial for increasing both ductility and strength of magnesium alloys. Equal channel angular pressing (ECAP) [8] is considered as the most popular SPD technique for producing of bulk ultrafine-grained materials. In this technique the material is severely deformed by repetitive pressing through a die consisting of two intersecting channels of the same cross section. In addition to substantial grain refinement, ECAP processing of Mg alloys usually yields a development of a strong texture, which significantly influences the ductility, the proof stress and the tensile strength of materials [9,10]. It is well known, that the texture strongly depends on the deformation route which is characterized by the angle and direction of sample rotation between consecutive passes [11]. However, the knowledge about the influence of ECAP processing temperature on the evolution of microstructure and texture in Mg

* Corresponding author. Charles University, Faculty of Mathematics and Physics, Ke Karlovu 3, 121 16 Praha 2, Czech Republic.
E-mail address: tomas.krajnak@karlov.mff.cuni.cz (T. Krajňák).

http://dx.doi.org/10.1016/j.jallcom.2017.02.061
0925-8388/

alloys is still limited [12]. Furthermore, only a small number of papers has been published about the properties of ultrafine-grained Mg-Al-Ca alloys. Some of them describe the microstructure, texture and mechanical properties of AZ31 magnesium alloy with 1 wt% Ca addition processed by hot extrusion and high-ratio differential speed rolling (HRDSR) [13,14]. In the present paper, we focus on the difference between the microstructures developed in extruded AX41 magnesium alloy processed by ECAP at temperatures of 220 °C and 250 °C. Particular attention is paid to the evolution of texture during ECAP processing. The behavior of the materials under uniaxial loading at RT is discussed on the basis of the microstructural characterization performed by electron backscatter diffraction (EBSD) and X-ray line profile analysis.

2. Experimental procedures

Commercial AX41 magnesium alloy (Mg - 4 wt% Al - 1 wt% Ca) was processed by the combination of hot extrusion and ECAP. Extrusion was performed at 350 °C and a speed of 60 mm/min, employing extrusion ratio (ER) of 19:1. ECAP processing was conducted at temperatures of 220 °C and 250 °C using a pressing velocity of 20 mm/min via route Bc, i.e., the samples were rotated by 90° in the same direction between consecutive passes. Billets with the length of 100 mm were pressed through a die with an internal channel angle of 90° and a cross section of 10 × 10 mm^2. Prior to each pass, the samples were preheated inside the incoming ECAP channel for 5 min. After each pass, the specimens were quenched into water. The ECAP processing was carried out by 1, 2, 4 and 8 passes. The samples were labeled according to the number of the applied ECAP passes and the temperature of processing. For instance, the specimen processed by 4 passes at 220 °C is labeled as 4P-220.

The characterization of the microstructure of the ECAP processed materials was carried out on the cross sections of the specimens (plane X) [15] lying perpendicular to the pressing direction by EBSD and X-ray line profile analysis. Prior to the measurements, the samples were polished to a mirror like surface quality using diamond suspensions. The finest suspension contained particles with the size of 250 nm. For EBSD investigations, the mechanically polished surface was ion milled using a Gatan PIPS™ ion mill at 2 kV and an incidence angle of 4°. For X-ray diffraction experiments, the mechanically polished surface was etched by a solution of 10 ml acetic acid, 4.2 g picric acid, 10 ml H_2O and 70 ml of ethanol for 20 s. The microstructure was examined by a Quanta FEG scanning electron microscope operated at 10 kV. The investigated area was 300 × 250 μm^2 and 100 × 100 μm^2 with the step size of 300 nm and 100 nm for the extruded and the ECAP processed samples, respectively. For X-ray line profile analysis, the diffraction patterns were measured by a high-resolution rotating anode diffractometer (type: RA-MultiMax9, manufacturer: Rigaku) using $CuK_{\alpha 1}$ (wavelength: $\lambda = 0.15406$ nm) radiation. The X-ray diffraction patterns, covering a diffraction angle range between 30 and 135°, were evaluated by Convolutional Multiple Whole Profile (CMWP) fitting method [16].

The mechanical properties were studied by uniaxial tension at RT and a constant strain rate of 10^{-4} s^{-1}. Dog bone shaped tensile specimens were machined according to ISO 527-2-5B and deformed by a universal Instron 5882 testing machine. The loading axis was parallel to the pressing direction of the last ECAP pass.

3. Experimental results

3.1. Microstructure from EBSD

The EBSD images in Fig. 1 reveal that the microstructure of the extruded alloy (EX) is homogeneous and consists of equiaxed grains with an average grain size of about 10 μm. The extruded sample exhibits a $\langle 10\bar{1}0 \rangle$ fiber texture (see Fig. 1c) which is typical for magnesium alloys processed by hot extrusion.

The EBSD images in Fig. 2 illustrate the refinement of the microstructure with increasing number of ECAP passes at 220 and 250 °C. At 220 °C, a gradual refinement of the microstructure was observed up to 4 passes, resulting in a very fine and homogeneous microstructure consisting of equiaxed grains. In contrast, at 250 °C fully refined homogeneous microstructure is formed even after 2 passes. After 4 passes a grain growth was observed and the microstructure remained almost unchanged during further processing (up to 8 passes). As a result, the microstructure of sample 8P-250 is coarser than that of the sample 8P-220.

The evolution of the mean grain size (determined as the area-weighted mean grain size from the EBSD images) and the fraction of high-angle grain boundaries (HAGBs), having misorientations higher than 15°, with increasing number of ECAP passes (N) are plotted in Fig. 3. The mean grain size gradually decreases up to the fourth and the second passes at 220 °C and 250 °C, respectively (see Fig. 3a). Further processing at 250 °C leads to a slight increase of the grain size to the value of 4.0 μm (sample 8P-250) while at 220 °C the grain size saturates at 2.7 μm (sample 8P-220). The fraction of HAGBs at 220 °C gradually increases with increasing N and saturates after 4 passes at the value of 82%. The same fraction of HAGBs was obtained even after 2 passes at 250 °C; however, after 8 passes its value drops to 70%.

3.2. Texture evolution determined by EBSD

The evolution of texture with increasing number of ECAP passes is described by a series of (0001) EBSD pole figures (see Fig. 4). The pole figures are orientated according to the orthogonal sample coordinate system shown in Fig. 5, where the x-axis is parallel to the pressing or extrusion direction.

After the first ECAP pass at 220 °C the fiber texture developed during extrusion is transformed into two strong texture components. One texture component, denoted as A, corresponds to the case when the basal planes are lying parallel to plane Z. In the second texture component (denoted as B) the basal planes are tilted by approximately 45° to the pressing direction (x-axis), i.e., the basal planes are parallel to the plane of the ECAP die channel intersection. From the second pass, both texture components were preserved; however, component B is additionally tilted roughly by 40° towards the y-axis. At 250 °C qualitatively similar texture evolution was observed, however after 8 passes the intensity of texture component B increases at the expense of texture component A. Thus, in 8P-250 sample the texture component B becomes dominant. For completeness of the texture investigation, the EBSD $\left(10\bar{1}0\right)$ pole figures for the samples processed by 8 passes at 220 and 250 °C are plotted in Fig. 6. The majority of prismatic planes is tilted by 45° towards the z-axis and simultaneously rotated randomly around the crystallographic c-axis in both samples. The validity of EBSD texture observation in 8P-220 sample was confirmed by X-ray diffraction measurement in a recently published paper by Krajnak et al. [17].

3.3. Microstructure study by X-ray line profile analysis

X-ray diffraction (XRD) analysis was performed in order to determine the phase compositions in the extruded and ECAP processed alloys. Fig. 7a shows an XRD pattern for the extruded sample (EX) which indicates that the microstructure before ECAP consists of a magnesium matrix and a eutectic Al_2Ca Laves phase, similarly

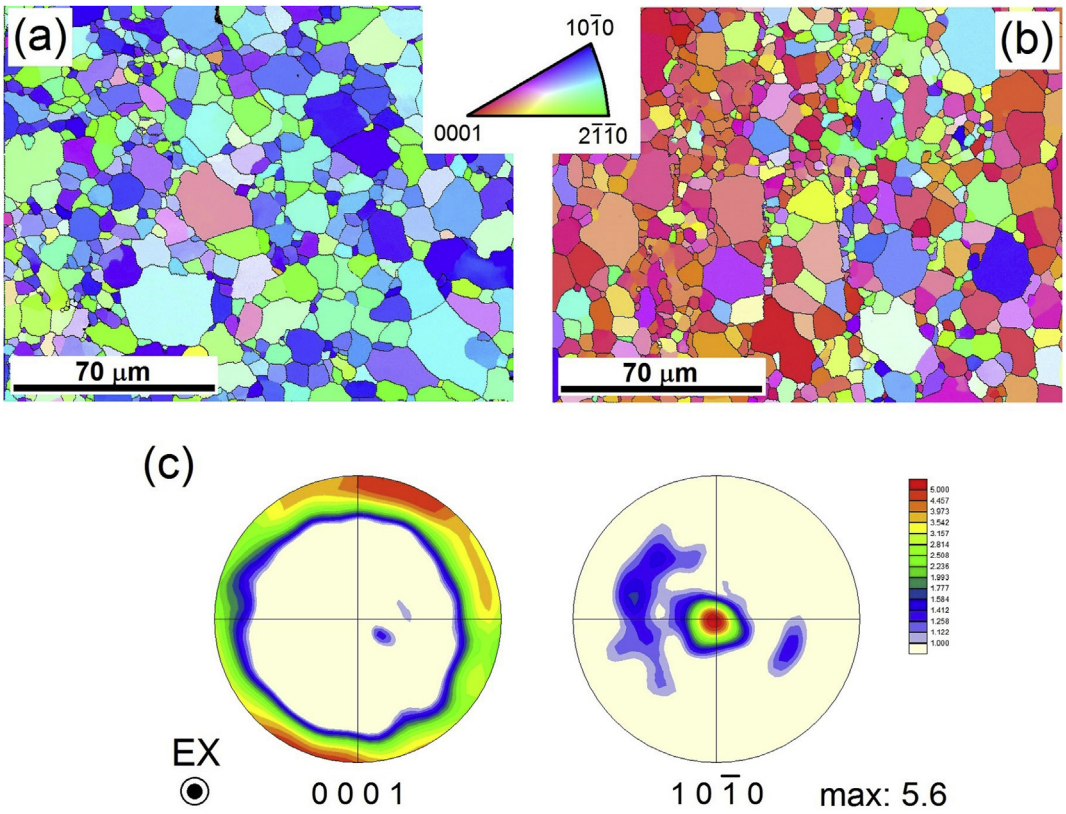

Fig. 1. EBSD inverse pole figure maps for (a) the cross and (b) the longitudinal sections of the extruded sample. (0001) and $\left(10\bar{1}0\right)$ pole figures obtained on the cross section are shown in (c).

to the as-cast state [5]. On the other hand, ECAP processing at both temperatures of 220 and 250 °C resulted in the formation of an additional $Mg_{17}Al_{12}$ phase, as shown in Fig. 7b. The XRD patterns for the samples ECAP processed at 250 °C are similar to those obtained at 220 °C, therefore they are not presented here. The relative intensities of the peaks varied with increasing number of passes due to the change of the texture and the fractions of the different phases. After ECAP processing by the highest number of passes (8P), no difference in the fraction of $Mg_{17}Al_{12}$ phase was observed for the two temperatures. In order to check the role of ECAP in the precipitation of $Mg_{17}Al_{12}$ phase, additional extruded samples were simply annealed at 220 and 250 °C for 20 min which is the approximate time of ECAP processing by 2 passes. As an example, the XRD pattern for the extruded specimen annealed at 220 °C for 20 min (EX-annealed) is shown in Fig. 7a. The XRD pattern of the extruded sample annealed at 250 °C for 20 min is not presented, as it is similar to that obtained after annealing at 220 °C. Peaks of $Mg_{17}Al_{12}$ phase were not observed in the simply annealed samples, which proves the significant role of ECAP straining in the development of these precipitates.

The dislocation density (ρ) as well as the median (m) and the log-normal variance (σ^2) of the log-normal crystallite size distribution function were obtained from the CMWP fitting of the diffraction patterns. Furthermore, the area-weighted mean crystallite size ($\langle x\rangle_{area}$ - i.e. the size of coherently scattering domains) was calculated as [16]:

$$\langle x\rangle_{area} = m \times \exp\left(2.5\sigma^2\right). \quad (1)$$

The dislocation density (ρ) and the area-weighted mean crystallite size as a function of ECAP passes are plotted in Fig. 8. The crystallite size and the dislocation density for the extruded sample (N = 0) were above and below the detection limits of the present XRD line profile analysis method (d > 1 μm, $\rho < 10^{13}$ m^{-2}). In Fig. 8, these respective limits were plotted for the extruded specimen (N = 0).

The evolution of the dislocation density with increasing number of ECAP passes is similar for both processing temperatures. However, at the lower temperature (220 °C) an approximately two times higher dislocation density was observed, cf. Fig. 8a. Even after the first pass of ECAP the dislocation density considerably increases. During further ECAP straining ρ decreases with increasing number of passes and reaches minimum values of ~0.7×10^{14} m^{-2} and ~0.4×10^{14} m^{-2} for samples 8P-220 and 8P-250, respectively. The reduction of the dislocation density from the second pass at both processing temperatures can be explained by the dynamic recovery and dynamic recrystallization [18]. At both temperatures the area-weighted mean crystallite size significantly decreases after 1 pass of ECAP to the value of ~200 nm and slightly increases after the second pass. After 4 passes at 250 °C, the crystallite size rapidly increases as a result of dynamic recovery and simultaneous coarsening of the microstructure; however, after 8 passes a similar value as for 250 °C was observed. The simultaneous decrease of the crystallite size and the fraction of high-angle grain boundaries between 4 and 8 ECAP passes at 250 °C suggest that the dislocations inside the grains were arranged into cell boundaries or walls, while the dislocation density remained unchanged. It should be noted, however, that the grain size determined by EBSD differs from the crystallite size, as the latter is equivalent to the size of coherently scattering domains and corresponds to dislocations cells or subgrains in SPD-processed metallic materials.

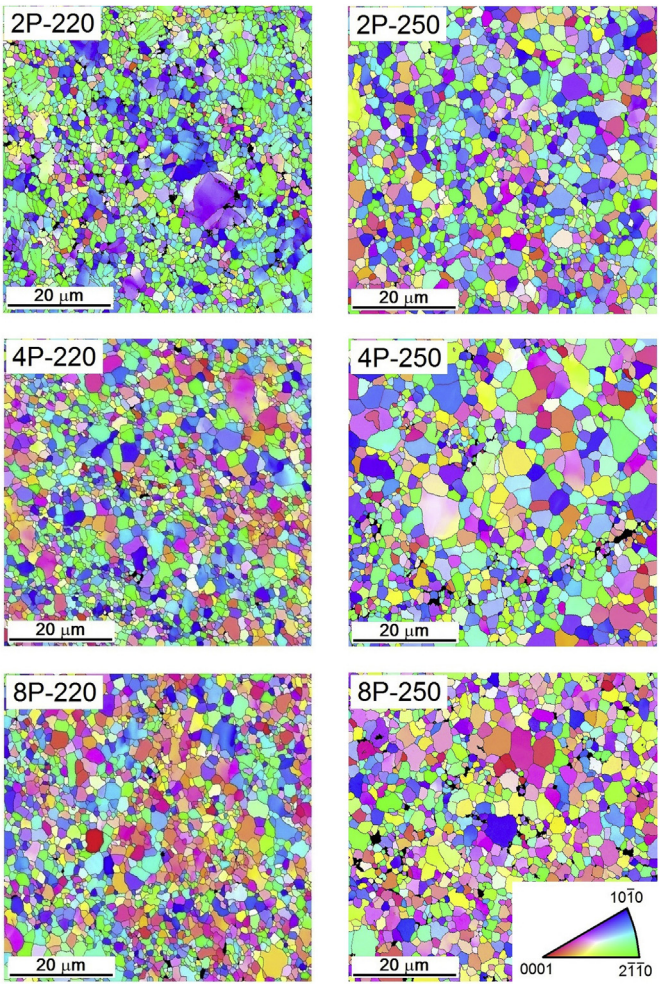

Fig. 2. EBSD inverse pole figure maps obtained on the cross sections of the samples processed by ECAP for different numbers of passes at 220 °C (left column) and 250 °C (right column).

Post-mortem analysis of the distribution of dislocations in the particular slip systems in the ECAP processed samples was estimated by the comparison of the experimentally determined dislocation contrast factors with the theoretical values, using the procedure described in detail in Ref. [19]. As the dislocation contrast factors of X-ray diffraction peaks for prismatic edge (PrE) and pyramidal edge (PyE) dislocations in <a>-type slip system family are close to each other [20], only the sum of their fractions is presented here. The majority of dislocations (70–90%) in all ECAP samples have <a>-type Burgers-vector. ECAP processing at 250 °C leads to a higher activation of basal slip in comparison to the processing at 220 °C and after 8 passes the fraction of basal edge (BE) dislocations is almost 5 times higher at 250 °C than at 220 °C (Fig. 9a). On the other hand, the fraction of PrE + PyE <a>-type dislocations at 250 °C is smaller than at 220 °C for large numbers of ECAP passes (see Fig. 9b). The fraction of the second order pyramidal edge $\{11\bar{2}2\}\langle 11\bar{2}\bar{3}\rangle$ <c+a> dislocations (Py2E) strongly varied as a function of the number of passes and the temperature of processing, see Fig. 9c. After 8 passes at 250 °C, the fraction of Py2E dislocations is approximately 4 times smaller in comparison to 8P-220 sample.

3.4. Room-temperature mechanical behavior obtained by tension

From the room-temperature tensile true stress-true strain curves the values of the proof stress (the value of true stress at the plastic strain of 0.2%) and the ductility (the maximum true strain at the necking of the sample) were evaluated. The evolution of the proof stress ($\sigma_{0.2}$) with increasing the number of ECAP passes is shown in Fig. 10a. At both processing temperatures, a significant increase of the proof stress after 1 pass is followed by a sharp drop after 2 passes. At 250 °C the proof stress further decreases up to 8 passes, while at 220 °C the proof stress remains high even after 8 passes. On the other hand, the ductility gradually increases up to 4 passes for both temperatures of processing, see Fig. 10b. The overall increases in ductility are about 35% and 50% for samples 8P-220 and 8P-250, respectively.

3.5. Calculation of Schmid factors for different slip systems activated during tension

The values of Schmid factors for uniaxial tension parallel to the x-axis for $\{0001\}\langle 11\bar{2}0\rangle$ basal, $\{10\bar{1}0\}\langle 11\bar{2}0\rangle$ prismatic and $\{11\bar{2}2\}\langle 11\bar{2}\bar{3}\rangle$ pyramidal slip systems were calculated from the EBSD data by software TSL OIM Analysis 7. The values of the calculated Schmid factors are summarized in Fig. 11. At both processing temperatures, the Schmid factor for basal slip (m_{basal}) gradually increases with increasing number of ECAP passes (N). For 2–8 passes, the samples processed at 250 °C exhibit higher values of m_{basal} in comparison with the specimens deformed by ECAP at

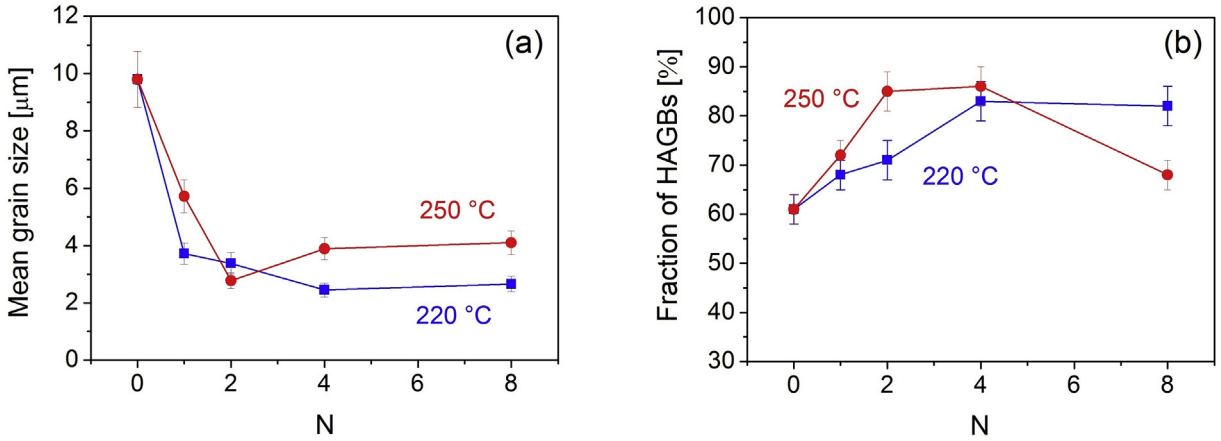

Fig. 3. The dependence of (a) the mean grain size and (b) the fraction of HAGBs on the number of ECAP passes (N) at 220 and 250 °C.

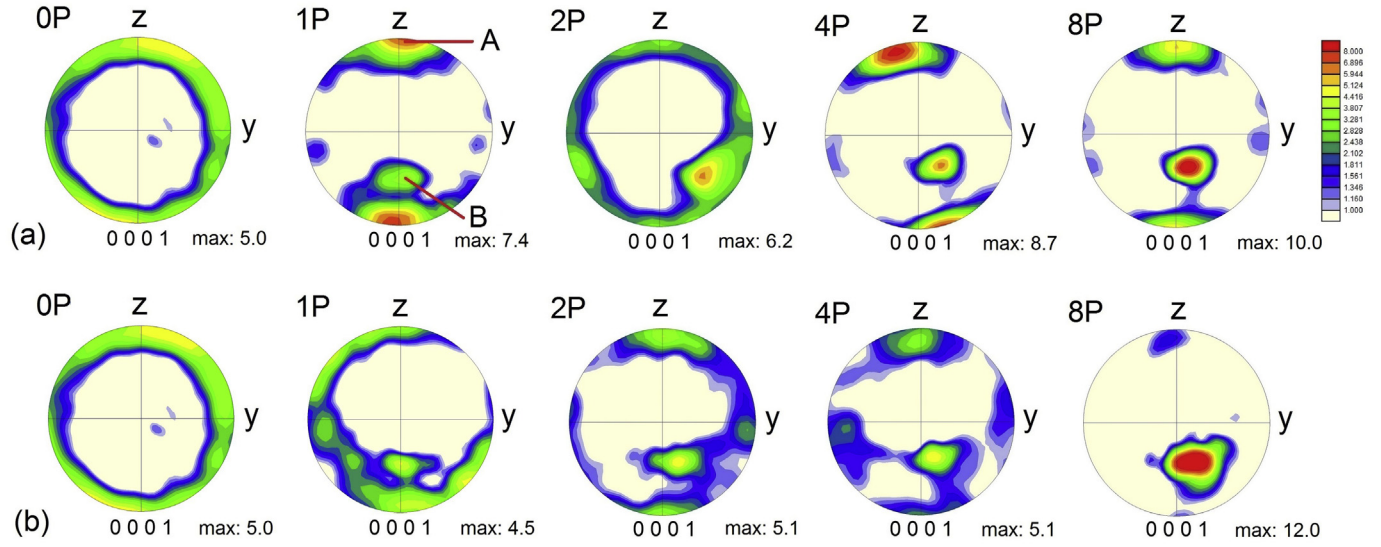

Fig. 4. EBSD (0001) pole figures for the samples processed by ECAP for different numbers of passes at (a) 220 °C and (b) 250 °C. The extruded sample before ECAP processing is labeled as 0P. The two main texture components developed during ECAP are denoted by A and B in the pole figure obtained for 1P at 220 °C.

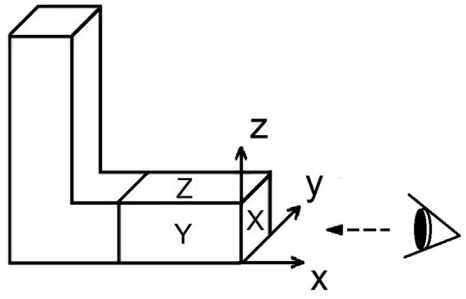

Fig. 5. Schematic representation of the sample coordinate system.

220 °C. After 8 passes, the overall increases in m_{basal} are about 180% and 220% for 220 and 250 °C, respectively, which leads to an easier activation of basal slip in comparison with the extruded state. The Schmid factors for the prismatic (m_{prism}) and the second order pyramidal (m_{pyram}) slip systems decrease with increasing number of ECAP passes and their values are the same for both processing temperatures, except for the samples processed by 2 passes. It is noted that the decrease of the values of m_{prism} and m_{pyram} (by about 25% after 8 passes) is much lower than the increase of m_{basal} (by about 200% after 8 passes).

4. Discussion

4.1. Microstructure evolution during ECAP performed at 220 and 250 °C

The grain refinement in magnesium alloys due to SPD usually occurred by the nucleation of fine grains along the preexisting grain boundaries [21]. The fragmentation of the microstructure during SPD is strongly influenced by the initial grain size. If the initial grain size is smaller than a critical value, d_c, a homogeneous microstructure is formed even after the first pass of ECAP. On the other hand, for grain sizes larger than d_c a bimodal grain structure develops, which gradually transforms to a homogeneous microstructure [22]. This critical grain size is between 3 and 9 μm for AZ31 alloy processed by ECAP at room temperature [22]. In that alloy, the bimodal grain size distribution developed during 1 pass disappears after 6 passes. However, the critical grain size depends on both alloy composition and ECAP conditions (e.g., on the temperature). The present microstructural observations indicate that the temperature of processing significantly influences the fragmentation rate of the microstructure in extruded AX41 magnesium alloy. For the processing temperature of 250 °C, a homogeneous fine-grained microstructure can be observed even after 2 passes, while for the temperature of 220 °C the microstructure becomes

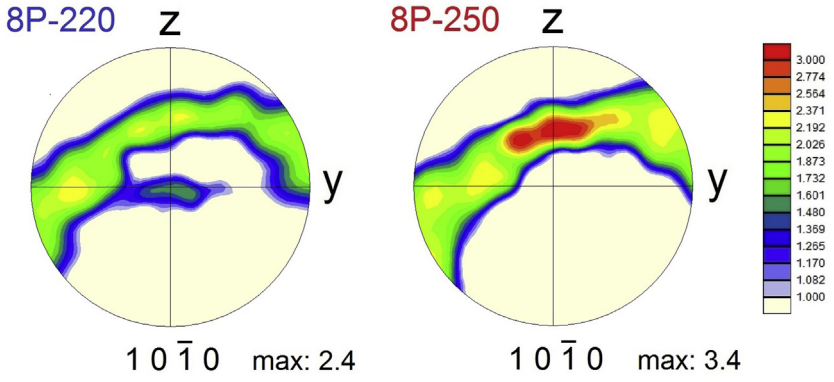

Fig. 6. EBSD$\left(10\bar{1}0\right)$ pole figures for the samples processed by 8 passes at 220 and 250 °C.

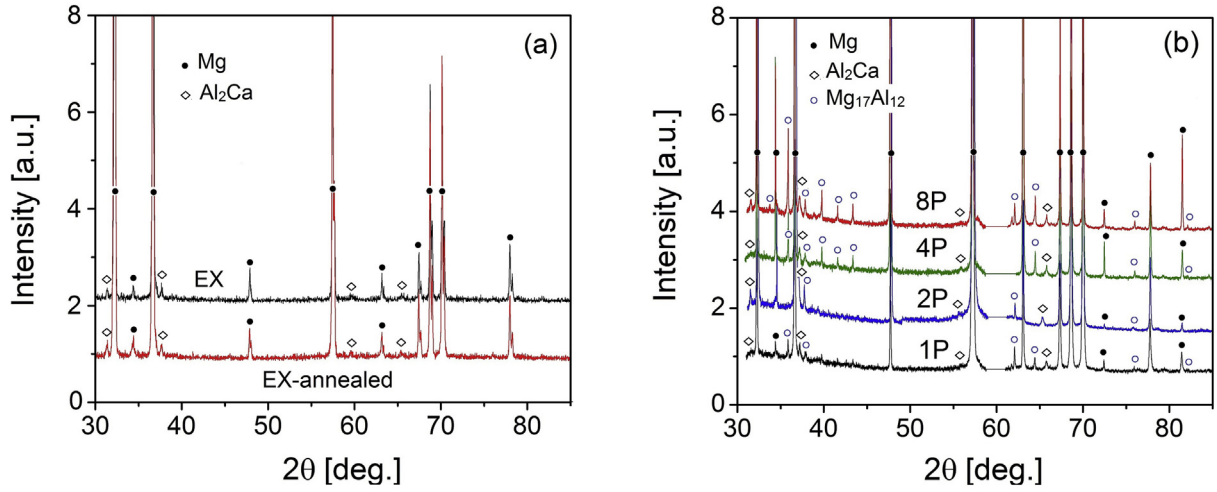

Fig. 7. (a) X-ray diffraction patterns of the extruded specimen (denoted as EX) and the sample extruded and then annealed at 220 °C for 20 min (denoted as EX-annealed). (b) X-ray diffractograms of the samples processed by ECAP by different passes at 220 °C.

homogeneous only after 4 passes. Due to the higher temperature of processing, the value of critical grain size increases and the homogeneous microstructure is achieved at lower number of passes. In other words, the overall fraction of dynamically recrystallized microstructure is influenced by the temperature of processing. This observation is consistent with the result of Beer et al. [23], who showed that the higher the temperature of hot compression is, the larger is the dynamically recrystallized volume in wrought AZ31 alloy. Similarly, Lin et al. [24] revealed that in ZA85 magnesium alloy the degree of dynamic recrystallization increased with increasing ECAP temperature as the microstructures obtained after 4 ECAP passes at 220 and 250 °C were more uniform than that developed at 180 °C.

This study demonstrates that ECAP processing at lower temperature results in a smaller average grain size, which is consistent with the observations of former studies [25,26]. Generally, the high stresses at the pre-existing grain boundaries result in a simultaneous activation of basal and non-basal slip systems which is necessary for the nucleation of new grains along the original grain boundaries [27]. The non-basal <a>-type dislocations have higher probability to lock each other and form dislocation tangles, compared to the basal ones. Thus, the higher fraction of non-basal dislocations (prismatic (PrE) and pyramidal (PyE) <a>-type dislocations) during 4 and 8 ECAP passes at 220 °C compared to 250 °C (see Fig. 9) increased the probability of new grain nucleation and facilitated the grain refinement at 220 °C [28]. Furthermore, coarsening of microstructure in 4P-250 sample can be explained by the reduced fraction of non-basal dislocations between 2 and 4 passes at 250 °C, which inhibits the nucleation of new grains and thus the high-temperature grain growth becomes dominant. The higher rate of recovery and recrystallization processes at the higher temperature most probably also contribute to the larger grain size achieved by ECAP processing at 250 °C.

In addition to the continuous refinement of the microstructure, a development of texture components A and B was also observed with increasing numbers of passes. The relative intensities of these two components were different at 220 and 250 °C. One basic mechanism of texture formation in magnesium alloys during ECAP is the rotation of the slip plane of prevailing slip system parallel to the theoretical shearing plane activated during ECAP. A detailed explanation of texture formation in AX41 magnesium alloy processed by different routes of ECAP was published recently in

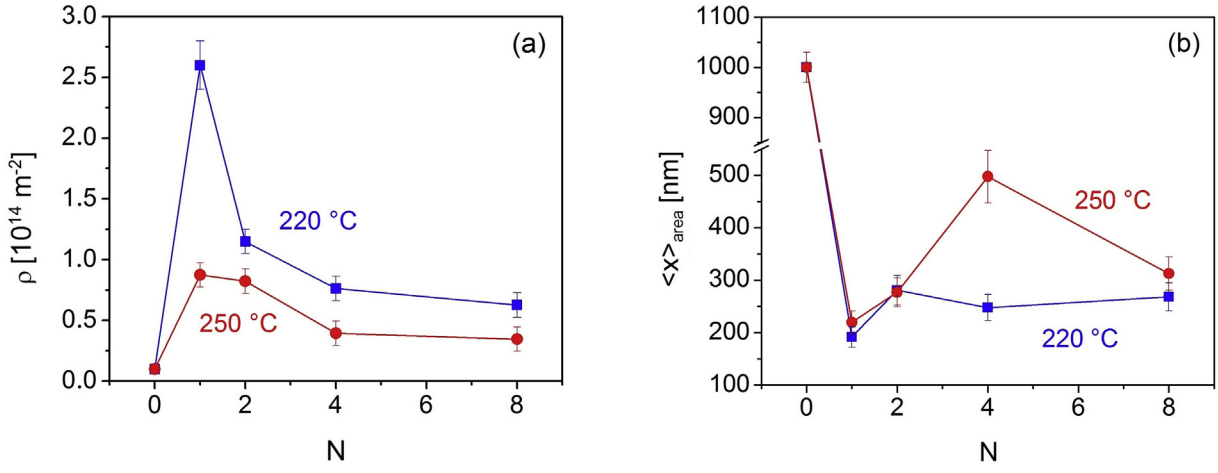

Fig. 8. Dependence of (a) the dislocation density and (b) the crystallite size on the number of ECAP passes at 220 and 250 °C.

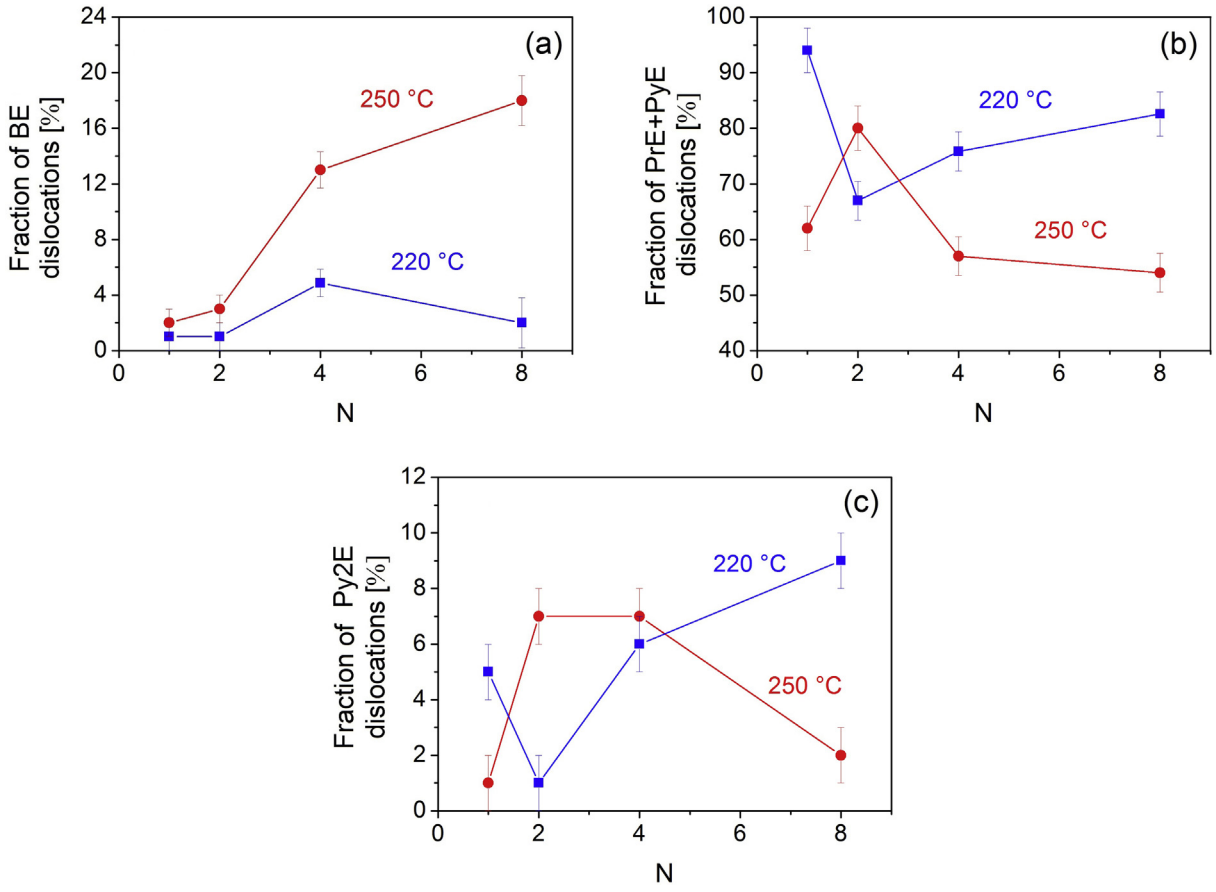

Fig. 9. The dependence of (a) the fraction of basal edge (BE) dislocations, (b) the sum of the fractions of prismatic (PrE) and pyramidal (PyE) <a>-type edge dislocations and (c) the fraction of the second order pyramidal edge (Py2E) <c+a> dislocations on the temperature of ECAP and the number of passes.

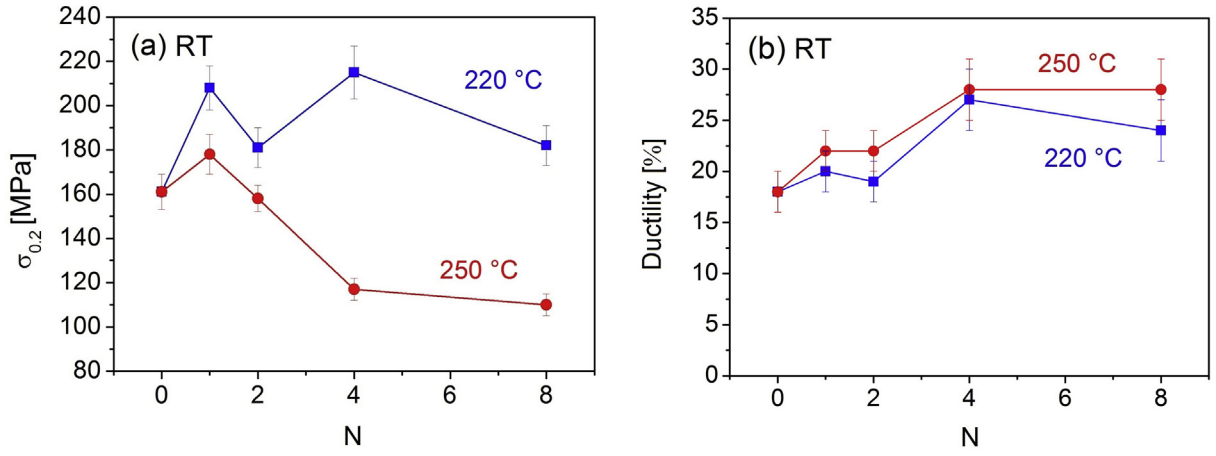

Fig. 10. Evolution of (a) the room-temperature proof stress and (b) ductility with increasing number of ECAP passes (N) at 220 and 250 °C.

Ref. [17]. The formation of texture component A is controlled by twinning, which occurs already in the feed-in channel, followed by the activation of the second order pyramidal slip system. This preserves the pyramidal planes $\{11\bar{2}2\}$ oriented parallel to the ECAP shearing plane. Moreover, the formation of texture component B is based on the activation of basal slip system, which causes the rotation of the (0001) basal planes parallel to the theoretical shearing plane of ECAP [29].

The post-mortem analysis of the Burgers vector population by X-ray line profile analysis showed that in all ECAP-processed samples the prismatic (PrE) and pyramidal (PyE) edge dislocations have the highest population (see Fig. 9), while the formation of texture component B required high activation of basal slip. This apparent discrepancy can be explained by the difference between the dislocations being active and stored during ECAP-processing. A fraction of active dislocations gliding through the grains may annihilate at grain boundaries and therefore do not contribute to the measured dislocation slip system population [30]. It is noted

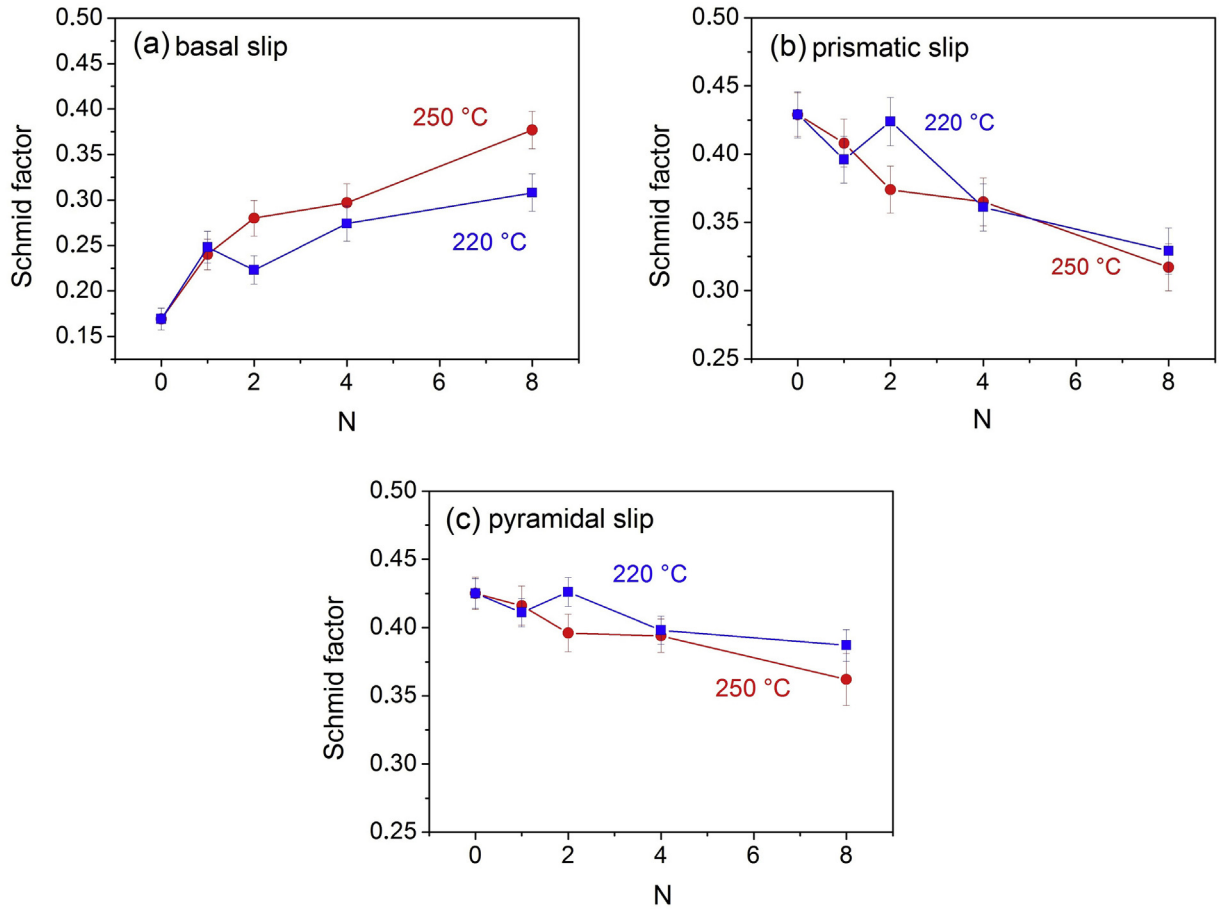

Fig. 11. The dependence of Schmid factors for (a) basal <a> slip, (b) prismatic <a> slip and (c) second order pyramidal <c+a> slip on the number of ECAP passes at 220 and 250 °C.

that the influence of ECAP temperature on the texture was also investigated formerly in pure magnesium processed via route A up to 8 passes [12]. It was found that with increasing temperature the intensity of the fibre texture component related to the activation of pyramidal <c+a> $\{2\bar{1}\bar{1}2\}\langle\bar{2}113\rangle$ slip system gradually increased and at 200 °C its intensity was higher than the intensity of the fibre texture component associated with the slip of basal $\{0001\}\langle 11\bar{2}0\rangle$ dislocations. On the other hand, a texture investigation in hot-extruded AZ31 processed by 4 passes via route Bc at 250 °C revealed the dominance of texture component B [11].

The higher temperature of plastic deformation usually yields a higher activation of <c+a> dislocations in polycrystalline samples with random crystallographic orientation. However, in our case the specimens processed by ECAP at two different temperatures exhibit different textures which influence the temperature dependence of the activation of basal and non-basal dislocations. Fig. 11 shows that due to the difference in texture the Schmid factor for basal slip is larger for 250 °C than 220 °C for N>1. Therefore, the basal slip is easier in specimens processed at 250 °C than at 220 °C. The higher activation of basal slip is consistent with the larger fraction of basal dislocations for 250 °C, as shown in Fig. 9a. It should be noted, however, that the fractions of the different types of dislocations obtained by X-ray line profile analysis reflect only the dislocation structure remained in the sample after ECAP processing and not the activities of the different slip systems. Although the activities of the different slip systems during ECAP certainly influence the fractions of the different dislocation types measured after deformation, they should not match exactly. For instance, the different annihilation rates of the various types of dislocations also have an effect on the populations of the slip systems. Indeed, Fig. 8 shows that for ECAP passes higher than 1 the dislocation density decreased due to the strongly active annihilation processes at the high temperatures of ECAP (at 220 and 250 °C). This observation suggests that the annihilation has an important role in the adjustment of the fractions of the different dislocation types observed after ECAP. Most probably, the annihilation of <c+a> dislocations is easier than <a> dislocations as the former dislocations have higher energy due to their longer Burgers vector. Therefore, the relative fraction of <c+a> dislocations measured after ECAP may be much lower than that estimated from their activity. The different annihilation rates of basal and non-basal dislocations, and the texture formation can explain the lower fraction of <c+a> dislocations for ECAP processing at 250 °C compared to processing at 220 °C.

In addition to the grain refinement and the texture evolution, the formation of $Mg_{17}Al_{12}$ precipitates was also observed even after the first pass of ECAP (which takes about 10 min) at both processing temperatures. Such rapid precipitation can be attributed to the combined effect of the elevated temperature and the severe straining during ECAP. This assumption was confirmed by annealing the extruded sample for 20 min at both temperatures, which did not result in the formation of $Mg_{17}Al_{12}$ phase (see Fig. 7a). Whereas, strain induced dynamic precipitation (SIDP) was widely observed in steel and Al alloys [31,32], its occurrence in Mg alloys was reported only rarely. For instance, SIDP of $Mg_{17}Al_{12}$ phase was observed inside dynamically recrystallized (DRXed) grains formed during hot rolling in an extruded Mg-8Al alloy [33]. According to

the Xia et al. [34], the high densities of dislocations and vacancies formed during hot deformation enable a fast diffusion of alloying elements, which may cause a non-equilibration segregation of solute atoms. DRXed regions may become favorable sites for precipitation because these regions contain huge numbers of grain boundaries and vacancies which promote precipitation.

It should also be noted that Al_2Ca precipitates present already in the extruded state together with $Mg_{17}Al_{12}$ precipitates formed during ECAP processing can act as recrystallization nucleation sites, and therefore effectively increase the fragmentation rate of the microstructure during SPD. In addition, precipitates may have a pinning effect on grain boundaries, thereby impeding grain growth during high temperature ECAP processing. Such promoting effect of precipitates on grain refinement was observed by Minarik et al. [35]. It was reported that AE42 magnesium alloy with almost two times higher fraction of $Al_{11}RE_3$ precipitates as compared to AE21 alloy exhibited higher fragmentation rate of the microstructure during the early stage of ECAP processing, even if a similar average grain size of 1.5 μm was obtained after 8 passes in both alloys.

4.2. Correlation between the microstructure and the mechanical performance

The tensile tests showed that the temperature of processing significantly influences the room-temperature proof stress (see Fig. 10a). ECAP processing at 250 °C leads to lower values of proof stress for all numbers of passes compared to 220 °C, mainly due to the lower dislocation density and/or the larger grain size. Moreover, the proof stress decreases due to ECAP processing at 250 °C as compared to the extruded state, despite the increase of the dislocation density and the decrease of the grain size. This softening can be attributed to the change of the texture during ECAP which yields an increase of the basal Schmid factor (see Fig. 11a), i.e., the basal slip becomes easier. During ECAP processing at 220 °C, the increase of the basal Schmid factor is smaller, therefore the reduction of the grain size and the increase of the dislocation density can cause a moderate hardening due to ECAP (see Fig. 10a). A former study on an ultrafine-grained ZM21 alloy processed by a two-stage ECAP at 200 °C and 150 °C also revealed that the development of a particular texture may result in a decrease in the room-temperature proof stress [36].

5. Conclusions

The evolution of the microstructure, texture and mechanical properties of extruded AX41 magnesium alloy was investigated as a function of ECAP passes (up to 8) at two different processing temperatures of 220 and 250 °C. The following conclusions were drawn:

- The processing temperature significantly influenced the fragmentation rate of microstructure. A homogeneous grain structure was obtained even after 2 passes of ECAP at 250 °C while the homogeneous microstructure developed only after 4 passes for the processing temperature of 220 °C. The smallest average grain size with the value of ~2.7 μm was achieved after 8 passes at 220 °C. On the other hand, for specimen processed by 8 passes at 250 °C the grain size was ~4 μm.
- The higher processing temperature of 250 °C led to a lower dislocation density with the value of ~0.4×10^{14} m^{-2} after 8 ECAP passes while the dislocation density was ~0.7×10^{14} m^{-2} for 220 °C. After 8 passes, a similar crystallite size of about 300 nm was achieved at both processing temperatures.
- The textures formed after 8 passes were significantly influenced by the temperature of processing. At 220 °C the $\langle 10\bar{1}0 \rangle$ fiber texture originating from the extrusion is transformed into two strong texture components, denoted as A and B. Processing at 250 °C caused weakening of texture component A at the benefit of component B, which resulted in a higher Schmid factor for basal slip between 2 and 8 ECAP passes.
- Processing by 8 passes at 220 °C led to a higher value of the room-temperature proof stress compared to the sample deformed by ECAP at 250 °C. This difference can be explained by the smaller average grain size, the higher density of dislocations and the specific texture, which is less favorable for the activation of basal slip. After 8 passes at both temperatures a significant increase in ductility was observed.

Acknowledgment

This work was financially supported by the Czech Science Foundation under the project 14-36566G. J.G. acknowledges the financial support of the Hungarian Scientific Research Fund, OTKA, Grant no. K-109021.

References

[1] W. Blum, P. Zhang, B. Watzinger, B.V. Grossmann, H.G. Haldenwange, Comparative study of creep of the die-cast Mg-alloys AZ91, AS21, AS41, AM60 and AE42, Mater. Sci. Eng. A 509 (2001) 735–740.
[2] Y. Lü, Q. Wang, X. Zeng, W. Ding, C.H. Zhai, Y. Zhu, Effects of rare earths on the microstructure, properties and fracture behavior of Mg-Al alloys, Mater. Sci. Eng. A 278 (2000) 66–76.
[3] M. Yang, F. Pan, J. Zhang, J. Zhang, An analysis of the development and applications of current and new Mg-Al based elevated temperature magnesium alloys, Mater. Sci. Forum 488–489 (2005) 923–926.
[4] S.W. Xu, N. Matsumoto, K. Yamamoto, S. Kamado, T. Honma, Y. Kojima, High temperature tensile properties of as-cast Mg-Al-Ca alloys, Mater. Sci. Eng. A 509 (2009) 105–110.
[5] R. Ninomiya, T. Ojiro, K. Kubota, Improved heat resistance of Mg-Al alloys by the Ca addition, Acta Metall. Mater. 43 (1995) 669–674.
[6] Y. Terada, R. Sota, N. Ishimatsu, T. Sato, K. Ohori, A thousandfold creep strengthening by Ca addition in die-cast AM50 magnesium alloy, Metall. Mater. Trans. A 35 (2004) 3029–3032.
[7] M.O. Pekguleryuz, J. Renaud, Creep resistance in Mg-Al-Ca casting alloys, in: H. Kaplan, J. Hryn, B. Clow (Eds.), Megnesium Technology 2000, TMS, Nashville, 2000, pp. 279–284.
[8] V.M. Segal, Materials processing by simple shear, Mater. Sci. Eng. A 197 (1995) 157–164.
[9] S.X. Ding, W.T. Lee, C.P. Chang, L.W. Chang, P.W. Kao, Improvement of strength of magnesium alloy processed by equal channel angular extrusion, Scr. Mater. 59 (2008) 1006–1009.
[10] S.R. Agnew, J.A. Horton, T.M. Lillo, D.W. Brown, Enhanced ductility in strongly textured magnesium produced by equal channel angular processing, Scr. Mater. 50 (2004) 377–381.
[11] M. Gzyl, A. Rosochowski, R. Pesci, L. Olejnik, E. Yakuschina, P. Wood, Mechanical properties and microstructure of AZ31B magnesium alloy processed by I-ECAP, Metall. Mater. Trans. A 45 (2014) 1609–1620.
[12] S. Biswas, H.G. Brokmeier, J.J. Fundenberger, S. Suwas, Role of deformation temperature on the evolution and heterogeneity of texture during equal channel angular pressing of magnesium, Mater. Charact. 102 (2015) 98–102.
[13] W.J. Kim, Y.G. Lee, High-strength Mg–Al–Ca alloy with ultrafine grain size sensitive to strain rate, Mater. Sci.Eng. A 528 (2011) 2062–2066.
[14] W.J. Kim, G.E. Lee, J.B. Lee, Achieving low temperature superplasticity from Ca-Containing magnesium alloy sheets, Adv. Eng. Mater. 11 (2009) 525–529.
[15] Y. Iwahashi, J. Wang, Z. Horita, M. Nemoto, T.G. Langdon, The shearing characteristics associated with equal-channel angular pressing, Mater. Sci. Eng. A 257 (1998) 328–332.
[16] G. Ribárik, J. Gubicza, T. Ungár, Correlation between strength and microstructure of ball-milled Al-Mg alloys determined by X-ray diffraction, Mater. Sci. Eng. A 387–389 (2004) 343–347.
[17] T. Krajňák, P. Minárik, J. Gubicza, K. Máthis, R. Kužel, M. Janeček, Influence of equal channel angular pressing routes on texture, microstructure and mechanical properties of extruded AX41 magnesium alloy, Mater. Charact. 123 (2017) 282–293.
[18] J. Müller, M. Janeček, S. Yi, J. Čížek, L. Wagner, Effect of equal channel angular pressing on microstructure, texture, and high-cycle fatigue performance of wrought magnesium alloys, Int. J. Mater. Res. 100 (2009) 838–842.
[19] K. Máthis, K. Nyilas, A. Axt, I.C. Dragomír, T. Ungár, P. Lukáč, The evolution of non-basal dislocations as a function of deformation temperature in pure magnesium determined by X-ray diffraction, Acta Mater. 52 (2004) 2889–2894.
[20] I.C. Dragomir, T. Ungár, Contrast factors of dislocations in the hexagonal

crystal system, J. Appl. Cryst. 35 (2002) 556–564.
[21] S.X. Ding, C.P. Chang, P.W. Kao, Effects of processing parameters on the grain refinement of magnesium alloy by equal-channel angular extrusion, Metall. Mater. Trans. 40A (2009) 415–425.
[22] R.B. Figueiredo, T.G. Langdon, Principles of grain refinement in magnesium alloys processed by equal-channel angular pressing, J. Mater. Sci. 44 (2009) 4758–4762.
[23] A.G. Beer, M.R. Barnett, Microstructural development during hot working of Mg-3Al-1Zn, Metall. Mater. Trans. A Phys. Metall. .Mater. Sci. 38 (2007) 1856–1867.
[24] Ch Y. Lin, H.J. Tsai, Ch G. Chao, T.F. Liu, Effects of equal channel angular extrusion on the microstructure and high-temperature mechanical properties of ZA85 magnesium alloy, J. Alloy Compd. 530 (2012), 48–45.
[25] S. Seipp, M.F. Wagner, K. Hockauf, I. Schneider, L.W. Meyer, M. Hockauf, Microstructure, crystallographic texture and mechanical properties of the magnesium alloy AZ31B after different routes of thermo-mechanical processing, Int. J. Plast. 35 (2012) 155–166.
[26] M. Gzyl, A. Rosochowski, E. Yakushina, P. Wood, L. Olejnik, Route effects in I-ECAP of AZ31B magnesium alloy, Key Eng. Mater. 554–557 (2013) 876–884.
[27] A. Galiyev, R. Kaibyshev, G. Gottstein, Correlation of plastic deformation and dynamic recrystallization in magnesium alloy ZK60, Acta Mater. 49 (2001) 1199–1207.
[28] A. Galiyev, R. Kaibyshev, G. Gottstein, Correlation of plastic deformation and dynamic recrystallization in magnesium alloy ZK60, Acta Mater. 49 (2001) 1199–1207.
[29] T. Mukai, M. Yamanoi, H. Watanabe, K. Higashi, Ductility enhancement in AZ31 magnesium alloy by controlling its grain structure, Scr. Mater. 45 (2001) 89–94.
[30] T. Mayama, M. Noda, R. Chiba, M. Kuroda, Crystal plasticity analysis of texture development in magnesium alloy during extrusion, Int. J. Plast. 27 (2011) 1916–1935.
[31] M. Militzer, W.P. Sun, J.J. Jonas, Modelling the effect of deformation-induced vacancies on segregation and precipitation, Acta Metall. 42 (1994) 133–141.
[32] S. Zhao, C. Meng, F. Mao, W. Hu, G. Gottstein, Influence of severe plastic deformation on dynamic strain aging of ultrafine grained Al-Mg alloys, Acta Mater 76 (2014) 54–67.
[33] F. Guo, D. Zhang, X. Yang, L. Jiang, F. Pan, Strain-induced dynamic precipitation of $Mg_{17}Al_{12}$ phases in Mg-8Al alloys sheets rolled at 748K, Mater. Sci. Eng. A 636 (2015) 516–521.
[34] X. Xia, Q. Chen, K. Zhang, Z. Zhao, M. Ma, X. Li, Y. Li, Hot deformation behavior and processing map of coarse-grained Mg-Gd-Y-Nd-Zr alloy, Mater. Sci. Eng. A 587 (2013) 283–290.
[35] P. Minárik, R. Král, J. Čížek, F. Chmelík, Effect of different c/a ratio on the microstructure and mechanical properties in magnesium alloys processed by ECAP, Acta Mater. 107 (2016) 83–95.
[36] E. Mostaed, A. Fabrizi, D. Dellasega, F. Bonollo, M. Vedani, Microstructure, mechanical behaviour and low temperature superplasticity of ECAP processed ZM21 Mg alloy, J. Alloy Compd. 638 (2015) 267–276.